RSC Advances

PAPER

View Article Online
View Journal | View Issue

Cite this: *RSC Adv.*, 2023, **13**, 31632

High-efficiency all-fluorescent white organic light-emitting diode based on TADF material as a sensitizer

Jie Hua,[ab] Zhuolin Zhan,[b] Zeyuan Cheng,[b] Wanshan Cao,[b] Yuan Chai,[b] Xufeng Wang,[b] Chunyu Wei,[b] He Dong[b] and Jin Wang *[ab]

Received 20th August 2023
Accepted 12th October 2023

DOI: 10.1039/d3ra05680e

rsc.li/rsc-advances

The use of TADF materials as both sensitizers and emitters is a promising route to achieve high-efficiency all-fluorescent white organic light-emitting diodes (WOLEDs). In this study, the thermally-activated delayed-fluorescent (TADF) material DMAC-TRZ (9,9-dimethyl-9,10-dihydroacridine-2,4,6-triphenyl-1,3,5-triazine) was selected as a sensitizer for the conventional fluorescent emitter DCJTB (4-(dicyanomethylene)-2-*t*-butyl-6-(1,1,7,7-tetramethyljulolidyl-9-enyl)-4*H*-pyran), which was co-doped in a wide bandgap host of DPEPO (bis[2-(diphenylphosphino)phenyl]ether oxide) to fabricate WOLEDs. For the emitting layer of DPEPO:DMAC-TRZ:DCJTB, the DPEPO host can dilute the exciton concentration formed on the DMAC-TRZ sensitizer, which benefits the suppression of exciton quenching. The effect of the doping concentration of DCJTB on the carrier recombination and energy transfer process was investigated. With an optimized doping concentration of DCJTB as 0.8%, highly efficient WOLED was achieved with a maximum external quantum efficiency (EQE), power efficiency (PE), and current efficiency (CE) of 11.05%, 20.83 lm W^{-1}, and 28.83 cd A^{-1}, respectively, corresponding to the Commission Internationale de l′ Eclairage (CIE) coordinates of (0.45, 0.46). These superior performances can be ascribed to the fact that the hole-trapping effect of the emitter and Dexter energy transfer (DET) from sensitizer to emitter can be suppressed simultaneously by the extremely low doping concentration.

1. Introduction

White organic light-emitting diodes (WOLEDs) are known as one of the most promising technologies for informational displays and solid-state lighting because of their low energy consumption, high efficiency, feasible mechanical flexibility, and good color stability.[1–5] Especially, owing to the simple manufacturing process and low commercialization cost, WOLEDs with single emitting layer (EML) have attracted more attention recently. In general, the emitters in the EML of OLEDs can be divided into three classes: conventional fluorescent, phosphorescent, and thermally activated delayed fluorescence (TADF) emitters. Based on spin statistics, singlet excitons (S_1) and triplet excitons (T_1) are generated by carrier recombination with a ratio of 25 : 75 under electrical excitation.[6] Because only 25% of singlet excitons contribute to light emission, conventional fluorescent OLEDs show low efficiency. Although phosphorescent emitters, such as platinum and iridium complexes can realize high efficiency *via* the utilization of both singlet and triplet excitons to radiate, the heavy metal (Ir or Pt) in phosphorescent emitters can result in high cost and resource scarcity.[7,8] Owing to the small singlet–triplet energy gap (ΔE_{ST}), TADF emitters can provide a new up-conversion avenue (*i.e.*, reverse intersystem crossing, RISC) to harvest all the singlet and triplet excitons, achieving highly efficient fluorescent OLEDs.[9–11] Thereby, the internal quantum efficiency (IQE) of TADF-based OLEDs can increase to 100% in theory.[12] Monochromatic OLEDs based on TADF emitters have successfully implemented good external quantum efficiency (EQE) over 30% in recent reports.[13–15] However, the application of all-TADF WOLEDs with a single EML is restricted due to serious efficiency roll-off at high luminance and poor spectral stability induced by unbalanced radiative decays between short and long wavelength emitters.[16,17]

Recently, the rapid development of TADF materials provided a promising route to improve the efficiency of conventional fluorescent-based OLEDs by adopting TADF materials as sensitizers, which promotes the application of all-fluorescent WOLEDs in flat panel display and lighting products.[18–23] In TADF-sensitized fluorescent OLEDs, TADF materials with twisted electron donor–acceptor (D–A) structures possess ambipolar carrier transport ability, which benefits the improvement of the carrier balance. On the other hand, TADF as a sensitizer can help to separate the RISC of TADF material and light-emitting of fluorescent materials, and the efficient Förster energy transfer (FRET) from TADF sensitizer to

[a]*Key Laboratory of Functional Materials Physics and Chemistry of the Ministry of Education, Jilin Normal University, Siping 136000, China. E-mail: jwang@jlnu.edu.cn*
[b]*College of Information Technology, Jilin Normal University, Siping 136000, China*

fluorescent guest benefits to achieve excellent device performance. Ma and co-workers reported a TADF-sensitized red fluorescent OLED with maximum EQE of 13.0% using a green TADF material Pr-1 (10,10′-((9-methyl-9*H*-purine-2,6-diyl)bis(4,1-phenylene))bis(10*H*-phenoxazine)) as a sensitizer and fluorescent material DCJTB (4-(dicyanomethylene)-2-*t*-butyl-6-(1,1,7,7-tetramethyljulolidyl-9-enyl)-4*H*-pyran) as a red emitter.[14] Zhao and co-workers reported a series of all-fluorescence three-color WOLEDs based on an interlayer sensitization configuration, successfully acquiring EQE of 30.8% and ultrahigh power efficiency (PE) of 110.7 lm W^{-1}, EQE of 31.0%, and color rendering index of 93.[22,23] More importantly, researchers have demonstrated that TADF sensitizer can also act as the emitter simultaneously by modulating the Förster and Dexter interactions, which would contribute to the realization of white light in combination with the complementary emitter.[24–26] Song *et al.*[25] fabricated a WOLED adopting the TADF-sensitized single EML consisting of conventional yellow fluorescent TBRb (2,8-ditert-butyl-5,11-bis(4-*tert*-butylphenyl)-6,12-diphenyltetracene) and blue TADF sensitizer DMAC-DPS (bis[4-(9,9-dimethyl-9,10-dihydroacridine)phenyl] sulfone), realizing maximum EQE of 15.5%. Although some studies have been devoted to TADF-sensitized fluorescent OLEDs, reduction in the exciton loss is still required to be investigated since the triplet excitons on the fluorescent emitter can recombine through nonradiative transitions. Therefore, efforts are needed to understand the carrier recombination and energy transfer process, to realize high-efficiency fluorescent OLEDs and improve the practical applications of the device.

In this study, we selected TADF material DMAC-TRZ (9,9-dimethyl-9,10-dihydroacridine-2,4,6-triphenyl-1,3,5-triazine) with a broad blue emission at about 495 nm as a TADF sensitizer for conventional fluorescence DCJTB and fabricated WOLED with single EML constructed using a wide bandgap host doped with TADF sensitizer and fluorescence emitter. By controlling the doping concentration of DCJTB, high-efficiency WOLED was achieved with a maximum EQE of 11.05%, PE of 20.83 lm W^{-1}, CE of 28.83 cd A^{-1}, and Commission Internationale de L'Eclairage (CIE) coordinates of (0.45, 0.46). The energy transfer mechanism and charge trapping effect in the TADF-sensitized OLEDs are studied in detail.

2. Experimental section

Organic materials, including DPEPO (bis[2-(diphenylphosphino)phenyl]ether oxide), DMAC-TRZ, HAT-CN (dipyrazino[2,3-*f*:2′,3′-*h*] quinoxaline-2,3,6,7,10,11-hexacarbonitrile), TAPC (di-[4-(*N*,*N*-ditolyl-amino)-phenyl]cyclohexane), mCP (1,3-bis(carbazol-9-yl)benzene) and TmPyPB (1,3,5-tri(*m*-pyrid-3-yl-phenyl)benzene) were purchased from Lumtec Company, while the fluorescent material DCJTB was purchased from Xi'an Polymer Light Technology Co Ltd. All the devices were fabricated on indium tin oxide (ITO) glass substrates with a sheet resistance of 10 Ω square^{-1}. Prior to the device fabrication, the ITO glass substrates were cleaned repeatedly by ultra-sonication in acetone, ethanol, and deionized water, and then dried at 130 °C for 1 hour, and subjected to ultraviolet (UV) ozone treatment for 20 minutes. Finally, they were transferred to a high vacuum thermal evaporation system with a base pressure of about 3×10^{-4} Pa. An oscillating quartz thickness monitor was used to monitor the evaporation rates and thickness. The evaporation rates were about 0.5^{-1} Å s^{-1} for organic layers, 0.1 Å s^{-1} for liq (8-hydroxyquinolinolato-lithium), and 10 Å s^{-1} for Al. In addition, the organic thin film samples for optical measurements were prepared by depositing organic materials on quartz substrates in a high vacuum thermal evaporation system with a pressure lower than 5×10^{-4} Pa.

The current density–voltage–luminance (*J*–*V*–*L*) characteristics, EL spectra, and CIE color coordinates of all the devices were measured using a PR655 spectrometer. The device efficiency (*i.e.*, EQE, PE, and CE) was calculated from current density, luminance, and EL spectral data. The UV/vis absorption and photoluminescence (PL) spectra were collected on a Shimadzu UV-2700 spectrophotometer and a Horiba Jobin Yvon Fluorolog-3 spectro-fluorometer, respectively. All measurements were performed in room temperature without any protective coatings.

3. Results and discussion

For high-performance all-fluorescent WOLEDs, we designed the EML structure as DPEPO:DMAC-TRZ:DCJTB, where DPEPO is the host, fluorescent DCJTB is the doping guest to emit red light, and TADF material of DMAC-TRZ acts as a sensitizer and blue emitter. It has been reported that DMAC-TRZ possesses strong polarity and high photoluminescence quantum yield (PLQY = 84%) due to its donor–acceptor structure characteristics and higher singlet radiative rate k_r^s ($\sim 10^7$ s^{-1}).[27–29] Thus, the DMAC-TRZ is an excellent sensitizer for improving the device performance. However, it should be dispersed in a wide bandgap host to prevent self-quenching.[12,30] Herein, we chose DPEPO as the host for the DMAC-TRZ sensitizer due to its wide bandgap (4.3 eV) and high triplet energy (T_1 = 2.98 eV).[31] Fig. 1(a) depicts the molecular structure of the main organic materials DCJTB, DMAC-TRZ, and DPEPO used in this work.

In TADF-sensitized fluorescent OLEDs, it is important to suppress carrier recombination on the fluorescent emitter and Dexter energy transfer (DET) between the TADF sensitizer and the fluorescent emitter. Both processes are concerned with the doping concentrations of fluorescent materials. Therefore, we first fabricated four devices with different DCJTB doping concentrations in the DMAC-TRZ-sensitized devices. The structure was: ITO/HAT-CN (10 nm)/TAPC (30 nm)/mCP(10 nm)/DPEPO : DMAC-TRZ : DCJTB (1 : 50 wt% : *x*, 10 nm)/TmPyPB (40 nm)/Liq (1 nm)/Al (100 nm), in which ITO and Al acted as the anode and cathode, respectively, HAT-CN and Liq were used as the hole and electron injection layers, respectively, TAPC and TmPyPB were chosen to act as the hole and electron transporting layers, respectively, mCP was selected as the exciton-blocking layer. The device structure and the energy level diagram are shown in Fig. 1(b). The high doping concentration (50 wt%) of DMAC-TRZ is necessary to achieve efficient energy transfer and ensure adequate blue emission.[32] The doping

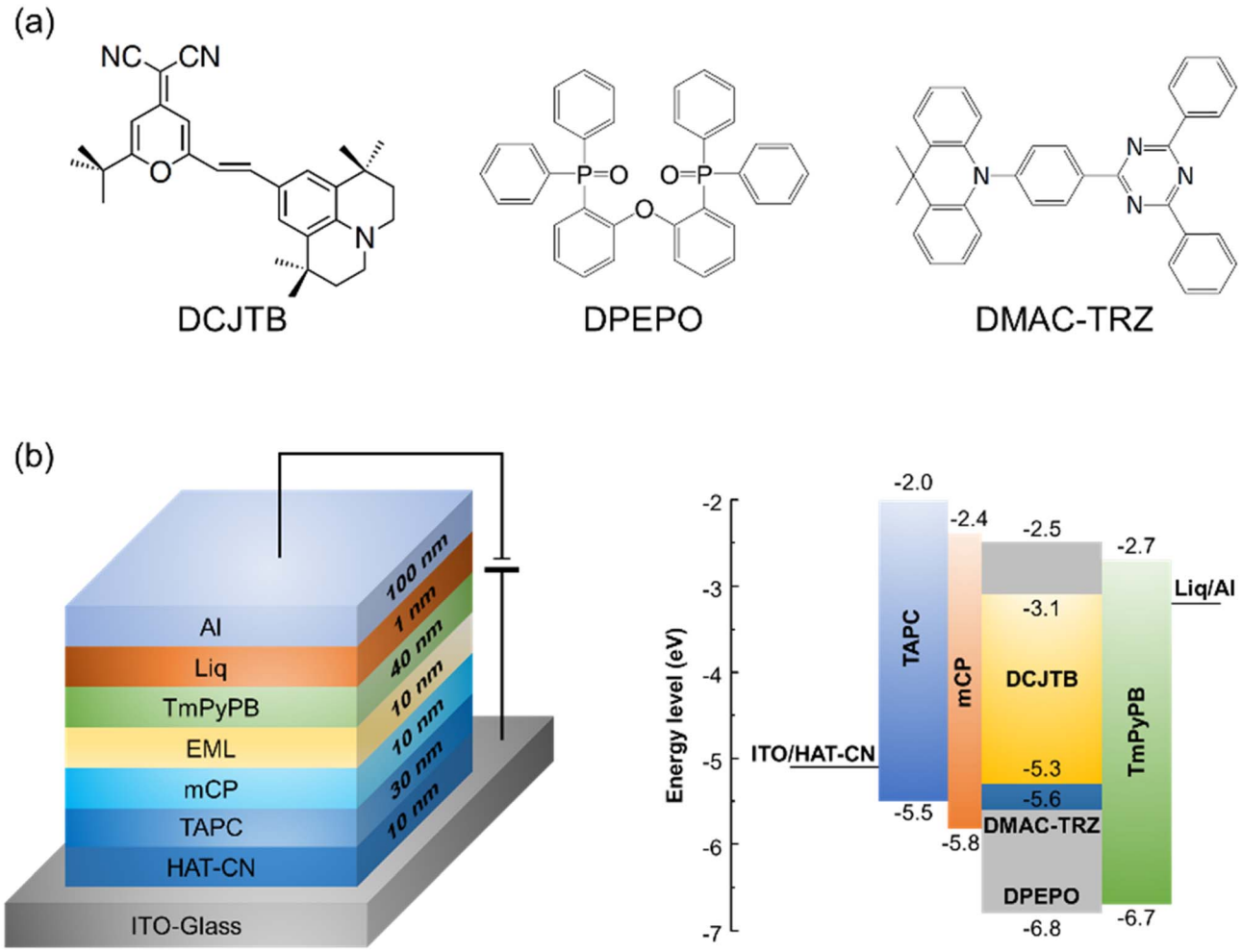

Fig. 1 (a) Chemical structures of DCJTB, DMAC-TRZ, and DPEPO molecules. (b) Structure and energy level diagram of the resulting TADF-sensitized OLEDs.

concentration x of DCJTB was set at 1.0, 1.5, 2.0, and 2.5 wt%, corresponding to devices A, B, C, and D, respectively.

Fig. 2 demonstrates the EL properties of devices A–D with various doping concentrations of DCJTB. The key EL parameters of these devices are summarized in Table 1. The normalized EL spectra (Fig. 2(a)) show that device A exhibits two peaks at 514 (blue-green) and 595 nm (red), which should have originated from DMAC-TRZ and DCJTB, respectively. The relatively low hole and electron mobilities of the DPEPO host result in a relatively high turn-on voltage for all devices A–D.[33] With increasing DCJTB doping concentration, the proportion of the blue-green emission from DMAC-TRZ gradually decreases and disappears in device D with 2.5 wt% doping concentration. In addition, owing to the concentration quenching induced by the strong intermolecular interaction of DCJTB, the EL peak of DCJTB is red-shifted from 595 to 620 nm with increasing doping concentration of DCJTB. The presence of blue-green emission from DMAC-TRZ in device A indicates the incomplete energy transfer process from DMAC-TRZ to DCJTB occurs, and the complete energy transfer can be observed in device D with 2.5 wt% doping concentration of DCJTB. However, it is worth noting that with an increasing doping concentration of DCJTB, some device performances such as current density, luminance, and efficiency (PE, CE, and EQE) show a remarkable reduction. As shown in Fig. 2(b)–(d) and Table 1, when the concentration of DCJTB increases, the turn-on voltage (V_{on}) manifests a gradual increase from 3.68 V for 1 wt% to 3.85 V for 2.5 wt%, and the current density at 9 V decrease from 72.9 mA cm^{-2} to 43.6 mA cm^{-2}. Simultaneously, the maximum luminance, PE, CE, and EQE decrease from 15 070 cd m^{-2}, 9.64 lm W^{-1}, 18.42 cd A^{-1}, and 7.15% to 3447 cd m^{-2}, 0.82 lm W^{-1}, 1.82 cd A^{-1}, 1.18%, respectively.

In DPEPO:DMAC-TRZ:DCJTB system, the lowest unoccupied molecular orbital (LUMO) and the highest occupied molecular orbital (HOMO) levels of DMAC-TRZ are −3.1 and −5.6 eV, respectively, which lie within those of the DPEPO, −2.5 and −6.8 eV, respectively. Holes and electrons recombine on DMAC-TRZ molecules directly to form the exciton after exciting optically or electrically, and then quickly transfer energy to DCJTB.[21] Thus, we fabricated a device using DPEPO : DMAC-TRZ (1 : 50 wt%) as EML. Fig. 3(a) depicts the normalized EL spectrum and EQE–J curve. As we expected, the devices emit single blue-green light at 516 nm from DMAC-TRZ, a high EQE of 10.41% can be ascribed to the suppression of the exciton quenching due

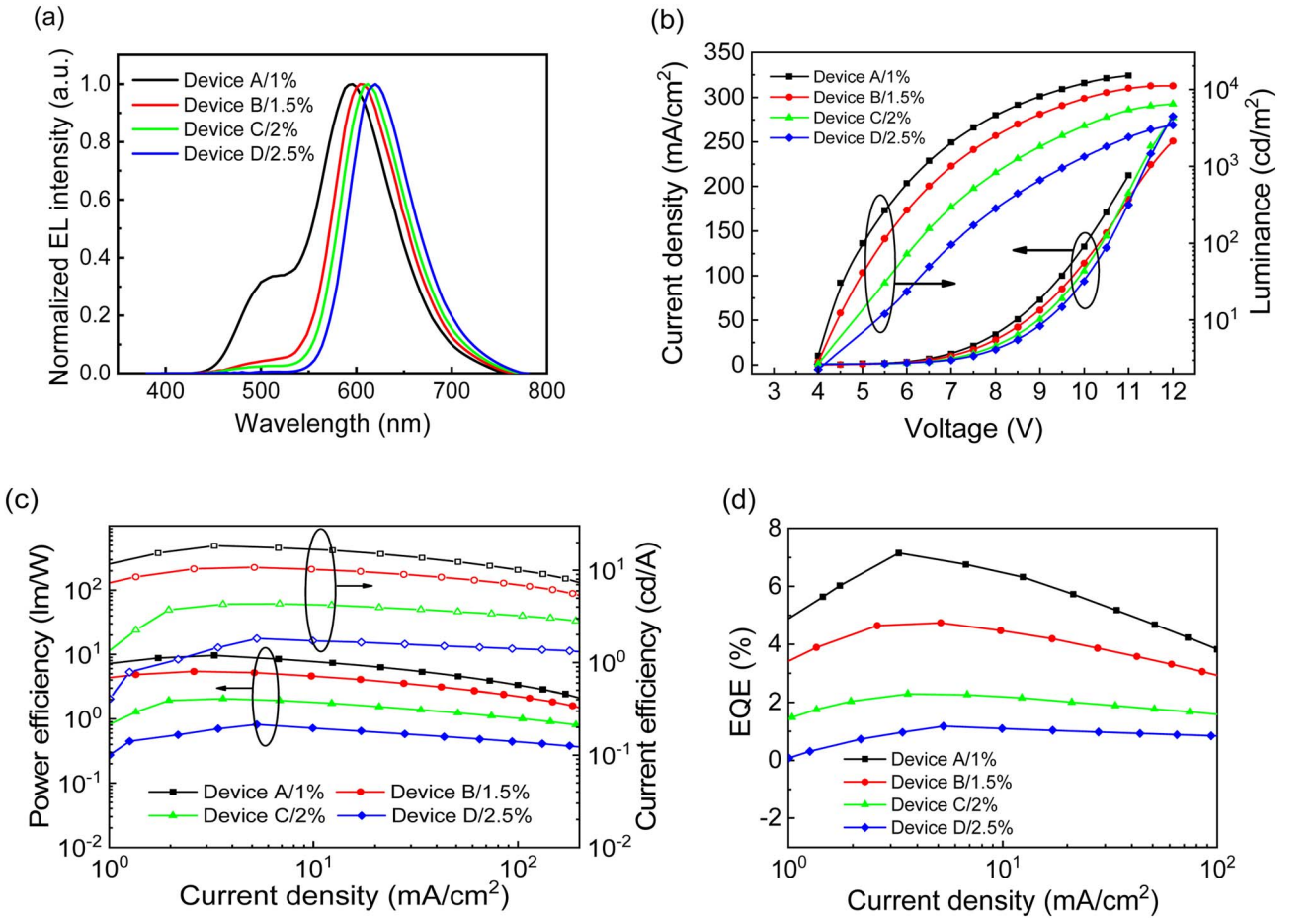

Fig. 2 EL performance of the devices A–D (a) the normalized EL spectra (at 20 mA cm^{-2}), and (b) current density–voltage–luminance (*J*–*V*–*L*) characteristics, (c) power efficiency and current efficiency *versus* current density characteristics (d) external quantum efficiency (EQE) *versus* current density characteristics.

to which the exciton concentration formed on DMAC-TRZ molecules is diluted by the DPEPO host. Furthermore, the photophysical behaviors of DMAC-TRZ and DCJTB neat films and their co-deposited films were also measured. As shown in Fig. 3(b), a larger spectral overlap between the absorption spectrum of DCJTB and the PL spectrum of DMAC-TRZ suggested that the effective FRET of singlet excitons from DMAC-TRZ to DCJTB can occur, including singlet excitons upconverted from the triplet state on the DMAC-TRZ molecules.[34] Moreover, two emissions from DMAC-TRZ and DCJTB can be detected from the PL spectrum of DMAC-TRZ:DCJTB co-deposited films and the emission intensity from DMAC-TRZ is apparently reduced as the DCJTB concentration increases from 1 wt% to 2 wt%. Those results also prove the occurrence of FRET from S_1 of DMAC-TRZ to S_1 of DCJTB. Fig. 3(c) and (d) show the transient PL decay for DMAC-TRZ and DCJTB neat films and DMAC-TRZ:DCJTB co-deposited film. The transient decay curves of DMAC-TRZ possess the prompt and delayed components with lifetimes of 24.2 and 858.5 ns for the neat DMAC-TRZ film, and 11.7 and 552.6 ns for DMAC-TRZ: DCJTB co-deposited films, respectively. Compared with the neat film, the exciton lifetimes of DMAC-TRZ are significantly shorter when doped

Table 1 EL parameters of devices A–D and device W

Device	V_{on}[a] (V)	EQE_{max} (%)	PE_{max} (lm W^{-1})	CE_{max} (cd A^{-1})	CIE coordinates[b]
A (1.0 wt%)	3.68	7.15	9.64	18.42	(0.45, 0.46)/(0.44, 0.47)
B (1.5 wt%)	3.75	4.74	5.42	10.75	(0.52, 0.43)/(0.51, 0.43)
C (2.0 wt%)	3.79	2.29	2.07	4.32	(0.58, 0.40)/(0.56, 0.41)
D (2.5 wt%)	3.85	1.18	0.82	1.82	(0.62, 0.37)/(0.59, 0.38)
W (0.8 wt%)	3.37	11.05	20.83	28.83	(0.45, 0.46)/(0.42, 0.47)

[a] Turn-on voltage. [b] Measured at maximum efficiency and 1000 cd m^{-2}, respectively.

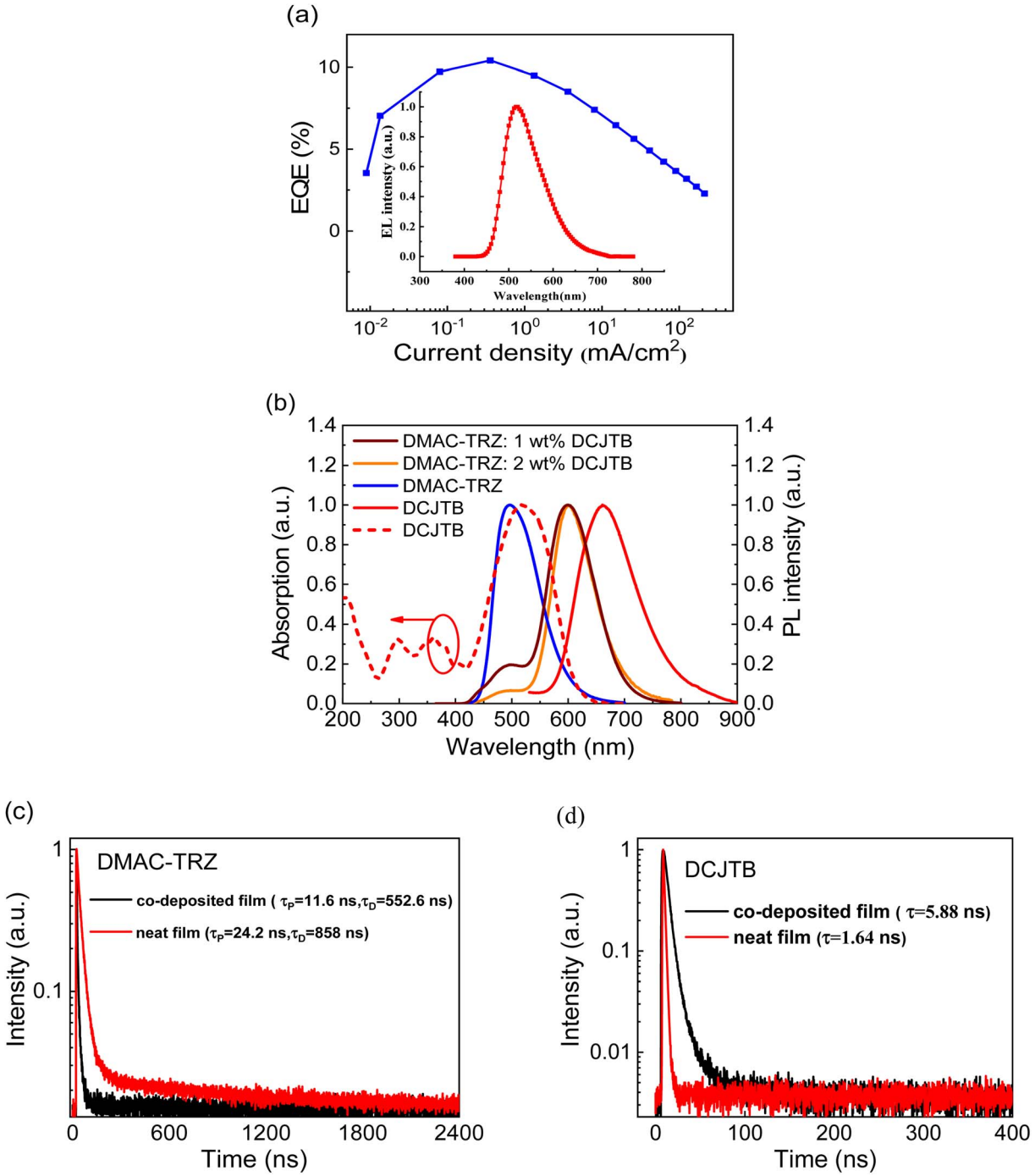

Fig. 3 (a) The EL properties of the device with DPEPO:DMAC-TRZ as EML, and (b) UV-absorption spectra (dotted lines) and PL spectra (solid lines), (c and d) time-resolved PL decay curves of DMAC-TRZ and DCJTB neat films as well as the DMAC-TRZ:DCJTB (1, 2 wt%) co-deposited film.

with 2 wt% DCJTB (shown in Fig. 3(b)), confirming that an additional decay process is induced by the efficient FRET of the singlet state on DMAC-TRZ, generated either directly or through the RISC process, to the DCJTB singlet state leading to a short lifetime of DMAC-TRZ. The energy transfer rate is calculated using the equation: $k_{ET} = 1/\tau_{D,A} - 1/\tau_D$, where $\tau_{D,A}$ and τ_D are the fluorescence lifetimes of DMAC-TRZ films with and without DCJTB, respectively. k_{ET} is calculated to be 3.49×10^7 s^{-1} for the prompt portion and 6.34×10^5 s^{-1} for the decayed portion. High k_{ET} benefits from the efficient RISC process of the triplet excitons induced by extremely small ΔE_{ST} (0.062 eV) of DMAC-TRZ through the upconverted process.[35] Additionally, the increase in the exciton lifetime of DCJTB from 1.64 ns for the neat film to 5.88 ns for the co-deposited films (Fig. 3(d)) further manifests that the energy transfer process leads to a rise in the exciton density in DCJTB molecules, which benefits to realize

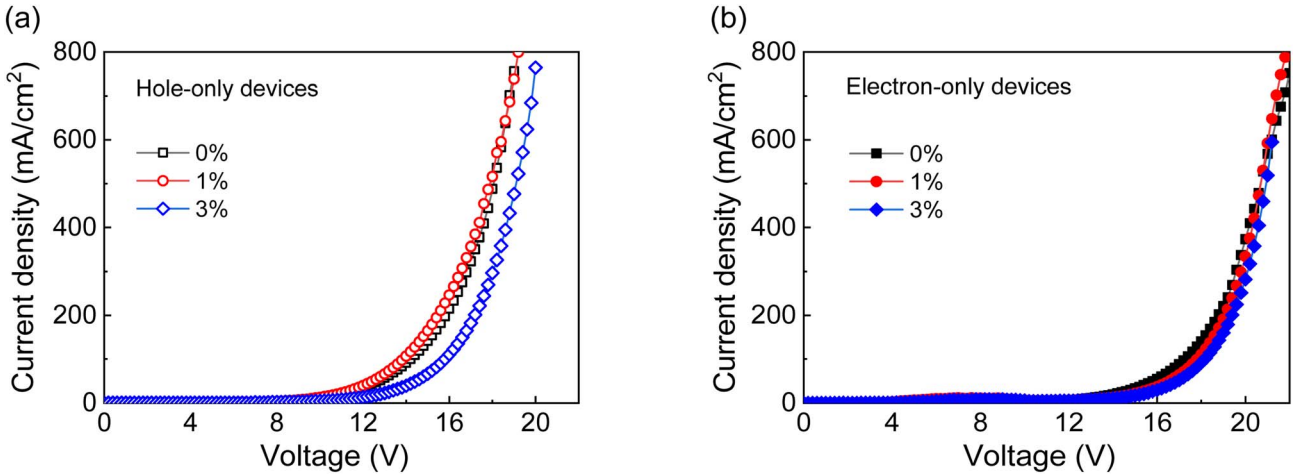

Fig. 4 The *J*–*V* characteristics of (a) hole-only (b) and electron-only devices with different concentrations of DCJTB.

high fluorescence efficiency. Unfortunately, compared with the device with DPEPO:DMAC-TRZ as EML, device A with DCJTB doped in EML of DPEPO:DMAC-TRZ shows low efficiency. Moreover, we did not observe high efficiency in devices B–D with increasing doping concentrations of DCJTB.

To explore the behavior underlying the reduced efficiency, we further fabricated the carrier-only devices to elucidate whether charge carrier trapping processes occur on DCJTB molecules in the resulting devices A–D. The detailed structure of the hole-only device was: ITO/HAT-CN(10 nm)/TAPC (30 nm)/mCP(10 nm)/DPEPO : DMAC-TRZ : DCJTB (1 : 50 wt% : *x*, 10 nm)/TAPC (30 nm)/HAT-CN (10 nm)/Al (100 nm), and the structure of the electron-only device was: ITO/Liq (1 nm)/TmPyPB (40 nm)/DPEPO : DMAC-TRZ : DCJTB (1 : 50 wt% : *x*, 10 nm)/TmPyPB (40 nm)/Liq (1 nm)/Al (100 nm), in which $x = 0$, 1 wt% and 3 wt. Fig. 4 shows the current intensity–voltage (*J*–*V*) characteristics of the hole- and electron-only devices with different concentrations of DCJTB. When the doping concentration of DCJTB increases from 0 to 1 wt%, the hole current density basically remained unchanged throughout the entire bias range from 0 to 17 V, but an obvious decrease can be observed when the doping concentration of DCJTB further increased to 3 wt% (Fig. 4(a)). This result indicates that in the DPEPO:DMAC-TRZ:DCJTB doping system, the hole trapping effect on DCJTB molecules can occur only when the doping concentration is larger than 1 wt% ($x > 1$ wt%), but it does not become an effective hole trap at low doping concentration ($x < 1$ wt%). While similar electron current densities are exhibited in the electron-only devices with various DCJTB doping

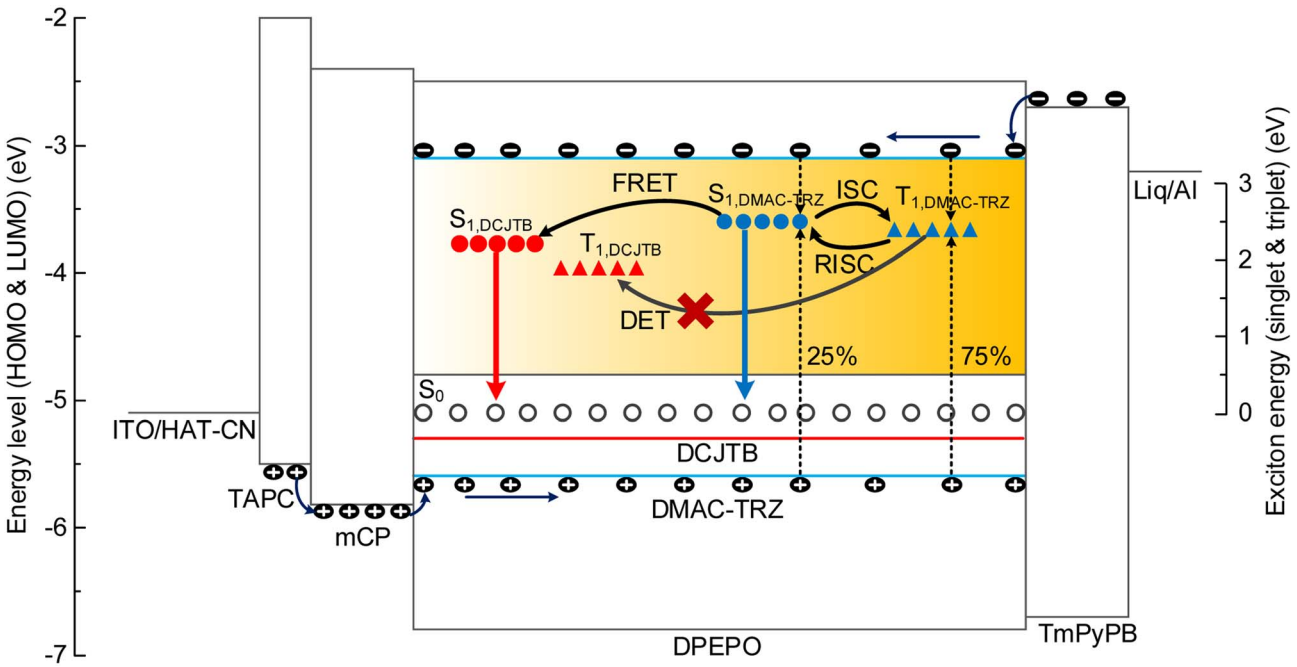

Fig. 5 Energy transfer processes in the DPEPO:DMAC-TRZ:DCJTB system at a low dopant concentration of DCJTB (<1 wt%).

concentrations from 0 to 3 wt% (Fig. 4(b)), also confirming that the electron trapping of DCJTB molecules is negligible. These can also be explained by the energy levels of the DPEPO:DMAC-TRZ:DCJTB doping system. As seen from the energy level diagram in Fig. 1(b), the LUMO level (3.1 eV) of DCJTB is almost equal to that of DMAC-TRZ, which can effectively suppress electron trapping. However, the HOMO level of DCJTB differs greatly from that of DMAC-TRZ by about 0.3 eV, which will increase the possibility of DCJTB as hole traps. On the other hand, high DCJTB doping concentration would decrease the intermolecular distance of DMAC-TRZ and DCJTB, leading to enhanced DET of the triplet excitons from the DMAC-TRZ sensitizer to the DCJTB emitter, thus restraining the RISC process on DMAC-TRZ molecule. These processes would lead to a certain extent of triplet exciton loss and a reduction in the efficiency of the fluorescent OLEDs at high doping concentrations.

In addition, to further clarify the exciton formation and energy transfer mechanism, the schematic diagram of the energy transfer and emission process is illustrated in Fig. 5. In the DPEPO:DMAC-TRZ:DCJTB system, the exciton concentration can be diluted by the introduction of the DPEPO host. Due to the high dopant concentration of DMAC-TRZ, the injected holes and electrons are mainly formed on DMAC-TRZ molecules, generating 25% singlet (S_1) and 75% triplet excitons (T_1). For the S_1 excitons of DMAC-TRZ, there are three possible decay pathways: (i) the S_1 excitons can transform immediately into the ground state (S_0) by emitting blue fluorescence. (ii) The S_1 excitons can be converted into the T_1 state of DMAC-TRZ *via* the intersystem crossing (ISC). (iii) The S_1 state transfer from DMAC-TRZ to DCJTB molecules *via* a long-range FRET, which can decay and produce red emission. On the other hand, the 75% T_1 excitons of DMAC-TRZ can be thermally upconverted into S_1 excitons through an efficient RISC process, resulting in the delayed fluorescence of DMAC-TRZ or go through the same FRET process, as mentioned above. Significantly, the direct charge trapping on the DCJTB molecules and unexpected DET between DMAC-TRZ to DCJTB emitter can be effectively suppressed due to the low concentration of DCJTB.[36,37] Therefore, the emission of fluorescent DCJTB is dominated by FRET from DMAC-TRZ.

In order to obtain high-efficiency WOLEDs, we further optimized the doping concentration of DCJTB to 0.8 wt%, and fabricated the device W with EML of DPEPO : DMAC-TRZ : DCJTB (1 : 50 wt% : 0.8 wt%, 10 nm). Fig. 6 shows the EL characteristics of device W, and the EL parameters are also summarized in Table 1. Compared with device A, the blue-green

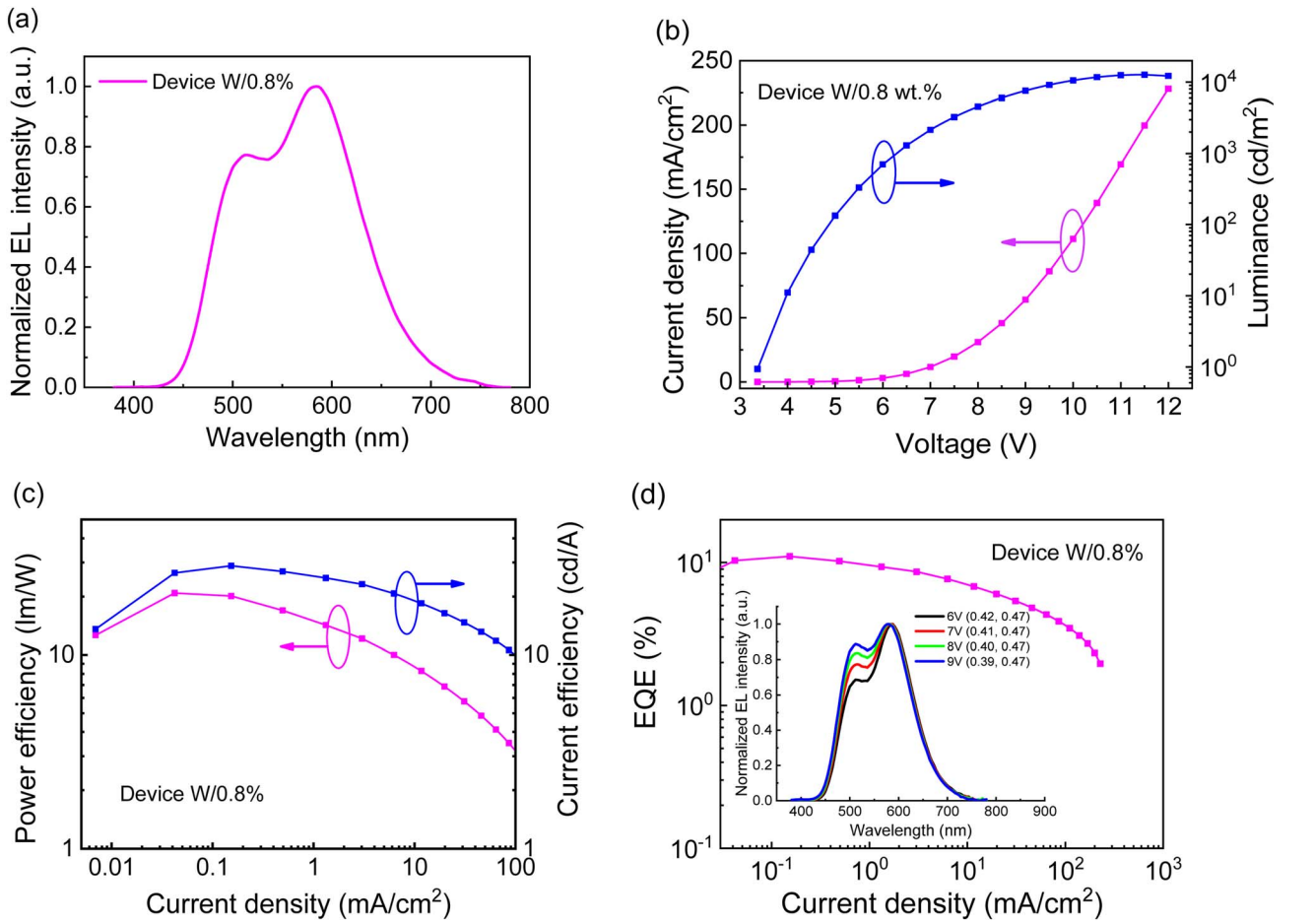

Fig. 6 (a) The normalized EL spectrum (at 20 mA cm^{-2}), (b) current density–voltage–luminance (*J*–*V*–*L*) characteristic, (c) power efficiency–current density–current efficiency (PE–*J*–CE) characteristics, (d) and external quantum efficiency–current density (EQE–*J*) characteristic of the device W.

emission intensity from DMAC-TRZ becomes stronger in device W. Furthermore, it forms a balanced white emission together with the red emission from DCJTB (Fig. 6(a)). Fig. 6(b) reveals a reduced turn-on voltage of 3.37 V and driving voltage of 6.26 V at 1000 cd m^{-2} (4.73 mA cm^{-2}). As shown in Fig. 6(c) and (d), the maximum EQE, PE, and CE of device W reach 11.05%, 20.83 lm W^{-1}, and 28.83 cd A^{-1}, respectively; at a typical display luminance of 100 cd m^{-2}, they remain as high as 9.74%, 15.33 lm W^{-1}, and 25.74 cd A^{-1}, respectively. The high efficiency can be attributed to the fact that singlet excitons of DMAC-TRZ are effectively transferred to DCJTB by the FRET process. Besides, the optimized device W also exhibits excellent EL spectral stability. As shown in the normalized EL spectra under different bias voltage (insert of Fig. 5(d)), the CIE coordinates change from (0.42, 0.47) at 700 cd m^{-2} (6 V) to (0.39, 0.47) at 7572 cd m^{-2} (9 V), and the *X* coordinate changes only 0.03, while the *Y* coordinate is basically unchanged. The slight increase in the blue-green intensity can be ascribed to the fact that the number of excitons that DCJTB can accept is limited due to the low doping concentration, and the excess excitons of DMAC-TRZ at high voltages were utilized for radiative decay.

4. Conclusions

We successfully fabricated high-efficiency all-fluorescent WOLEDs with a single EML by controlling the doping concentration of blue-green TADF sensitizer and conventional red fluorescent emitter employing a wide bandgap DPEPO host. Wide gap DPEPO can benefit from diluting the exciton concentration formed on DMAC-TRZ sensitizer. The hole-trapping effect on the DCJTB emitter and DET between DMAC-TRZ and DCJTB can be effectively suppressed at low doping concentrations. Consequently, the WOLEDs achieve high efficiency with a maximum EQE of 11.05%, power efficiency of 20.83 lm W^{-1}, and current efficiency of 28.83 cd A^{-1}. This work provides a feasible approach to fabricate high-performance WOLEDs with low cost and high efficiency based conventional fluorescent emitter, thus satisfying the commercial application.

Conflicts of interest

The authors declare no competing financial interest.

Acknowledgements

This work was supported by the Projects of the National Natural Science Foundation of China (11774134, 62374073), the Foundation of Science and Technology of Jilin, China (20220101041JC, 20230508058RC).

References

1 G. Schwartz, S. Reineke, T. C. Rosenow, K. Walzer and K. Leo, Triplet Harvesting in Hybrid White Organic Light-Emitting Diodes, *Adv. Funct. Mater.*, 2009, **19**, 1319–1333.
2 G. Shi, X. Zhang, M. Wan, S. Wang, H. Lian, R. Xu and W. Zhu, High-performance inverted organic light-emitting diodes with extremely low efficiency roll-off using solution-processed ZnS quantum dots as the electron injection layer, *RSC Adv.*, 2019, **9**, 6042–6047.
3 B. Liu, X. L. Li, H. Tao, J. Zou, M. Xu, L. Wang, J. Peng and Y. Cao, Manipulation of exciton distribution for high-performance fluorescent/phosphorescent hybrid white organic light-emitting diodes, *J. Mater. Chem. C*, 2017, **5**, 7668–7683.
4 M. Chapran, P. Pander, M. Vasylieya, G. W. Salyga, J. Ulanski, F. B. Dias and P. Data, Realizing 20% External Quantum Efficiency in Electroluminescence with Efficient Thermally Activated Delayed Fluorescence from an Exciplex, *ACS Appl. Mater. Interfaces*, 2019, **11**, 13460–13471.
5 X. Wei, L. Gao, Y. Miao, Y. Zhao, M. Yin, H. Wang and B. Xu, A new strategy for structuring white organic light-emitting diodes by combining complementary emissions in the same interface, *J. Mater. Chem. C*, 2020, **8**, 2772–2779.
6 M. A. Baldo, D. F. O'Brien, M. E. Thompson and S. R. Forrest, Excitonic singlet-triplet ratio in a semiconducting organic thin film, *Phys. Rev. B*, 1999, **60**, 14422–14428.
7 H. Sasabe, J. Takamatsu, T. Motoyama, S. Watanabe, G. Wagenblast, N. Langer, O. Molt, E. Fuchs, C. Lennartz and J. Kido, High-efficiency blue and white organic light emitting devices incorporating a blue iridium carbene complex, *Adv. Mater.*, 2010, **22**, 5003–5007.
8 M. Kim and J.-Y. Lee, Engineering the substitution position of diphenylphosphine oxide at carbazole for thermal stability and high external quantum efficiency above 30% in blue phosphorescent organic light-emitting diodes, *Adv. Funct. Mater.*, 2014, **24**, 4164–4169.
9 B. Li, Z. Li, T. Hu, Y. Zhang, Y. Wang, Y. Yi, F. Guo and L. Zhao, Highly efficient blue organic light-emitting diodes from pyrimidine-based thermally activated delayed fluorescence emitters, *J. Mater. Chem. C*, 2018, **6**, 2351–2359.
10 T. Ohsawa, H. Sasabe, T. Watanabe, K. Nakao, R. Komatsu, Y. Hayashi, Y. Hayasaka and J. Kido, A Series of Imidazo 1,2-f phenanthridine-Based Sky-Blue TADF Emitters Realizing EQE of over 20, *Adv. Opt. Mater.*, 2019, **7**, 1801282.
11 H. Wang, L. Xie, Q. Peng, L. Meng, Y. Wang, Y. Yi and P. Wang, Novel Thermally Activated Delayed Fluorescence Materials-Thioxanthone Derivatives and Their Applications for Highly Efficient OLEDs, *Adv. Mater.*, 2014, **26**, 5198–5204.
12 F. B. Dias, K. N. Bourdakos, V. Jankus, K. C. Moss, K. T. Kamtekar, V. Bhalla, J. Santos, M. R. Bryce and A. P. Monkman, Triplet Harvesting with 100% Efficiency by Way of Thermally Activated Delayed Fluorescence in Charge Transfer OLED Emitters, *Adv. Mater.*, 2013, **25**, 3707–3714.
13 H. Liu, Y. Fu, J. Chen, B. Z. Tang and Z. J. Zhao, Energy-Efficient Stable Hyperfluorescence Organic Light-Emitting Diodes with Improved Color Purities and Ultrahigh Power Efficiencies Based on Low-Polar Sensitizing Systems, *Adv. Mater.*, 2023, **35**, 2212237.
14 Y. Chen, D. D. Zhang, Y. W. Zhang, X. Zeng, T. Y. Huang, Z. Y. Liu, G. M. Li and L. Duan, Approaching Nearly 40% External Quantum Efficiency in Organic Light Emitting Diodes Utilizing a Green Thermally Activated Delayed

Fluorescence Emitter with an Extended Linear Donor-Acceptor-Donor Structure, *Adv. Mater.*, 2021, **33**, 2103293.

15 Y. Fu, H. Liu, B. Z. Tang and Z. J. Zhao, Realizing efficient blue and deep-blue delayed fluorescence materials with record-beating electroluminescence efficiencies of 43.4, *Nat. Commun.*, 2023, **14**, 2019.

16 C. Murawski, K. Leo and M. C. Gather, Efficiency Roll-Off in Organic Light-Emitting Diodes, *Adv. Mater.*, 2013, **25**, 6801–6827.

17 J. Yao, Z. Wang, X. Qiao, D. Yang, Y. Dai, Q. Sun, J. Chen, C. Yang and D. Ma, High efficiency and long lifetime fluorescent organic light -emitting diodes based on cascaded energy transfer processes to efficiently utilize triplet excitons via sensitizer, *Org. Electron.*, 2020, **84**, 105824.

18 D. Zhang, L. Duan, C. Li, Y. Li, H. Li, D. Zhang and Y. Qiu, High-Efficiency Fluorescent Organic Light-Emitting Devices Using Sensitizing Hosts with a Small Singlet-Triplet Exchange Energy, *Adv. Mater.*, 2014, **26**, 5050–5055.

19 B. Zhao, Y. Miao, Z. Wang, K. Wang, H. Wang, Y. Hao, B. Xu and W. Li, High efficiency and low roll-off green OLEDs with simple structure by utilizing thermally activated delayed fluorescence material as the universal host, *Nanophotonics*, 2017, **6**, 1133–1140.

20 D. Liu, K. Sun, G. Zhao, J. Wei, J. Duan, M. Xia, W. Jiang and Y. Sun, Spatial separation of a TADF sensitizer and fluorescent emitter with a core-dendron system to block the energy loss in deep blue organic light-emitting diodes, *J. Mater. Chem. C*, 2019, **7**, 11005–11013.

21 T. Higuchi, H. Nakanotani and C. Adachi, High-efficiency white organic light-emitting diodes based on A blue thermally activated delayed fluorescent emitter combined with green and red fluorescent emitters, *Adv. Mater.*, 2015, **27**, 2019–2023.

22 H. Liu, Y. Fu, B. Z. Tang and Z. J. Zhao, Realizing High Efficiency and High Color Quality for All-Fluorescence White Organic Light-Emitting Diodes by Interlayer-Sensitizing Configuration with Electron-Capturing Agent, *Adv. Funct. Mater.*, 2023, 2309770.

23 H. Liu, Y. Fu, B. Z. Tang and Z. J. Zhao, All-fluorescence white organic light-emitting diodes with record-beating power efficiencies over 130 lm W^{-1} and small roll-offs, *Nat. Commun.*, 2022, **13**, 5154.

24 B. Zhao, T. Zhang, W. Li, Z. Su, B. Chu, X. Yan, F. Jin, Y. Gao and H. Wu, Highly efficient and color stable single-emitting-layer fluorescent WOLEDs with delayed fluorescent host, *Org. Electron.*, 2015, **23**, 208–212.

25 W. Song, I. H. Lee, S.-H. Hwang and J. Y. Lee, High efficiency fluorescent white organic light-emitting diodes having a yellow fluorescent emitter sensitized by a blue thermally activated delayed fluorescent emitter, *Org. Electron.*, 2015, **23**, 138–143.

26 P. Wei, D. Zhang and L. Duan, Modulation of Forster and Dexter Interactions in Single-Emissive-Layer All-Fluorescent WOLEDs for Improved Efficiency and Extended Lifetime, *Adv. Funct. Mater.*, 2020, **30**, 1907083.

27 Y. Wada, K. Shizu, S. Kubo, T. Fukushima, T. Miwa, H. Tanaka, C. Adachi and H. Kaji, Highly efficient solution-processed host-free organic light-emitting diodes showing an external quantum efficiency of nearly 18% with a thermally activated delayed fluorescence emitter, *Appl. Phys. Express*, 2016, **9**, 032102.

28 F.-M. Xie, S.-J. Zou, Y. Li, L.-Y. Lu, R. Yang, X.-Y. Zeng, G.-H. Zhang, J. Chen and J.-X. Tang, Management of Delayed Fluorophor-Sensitized Exciton Harvesting for Stable and Efficient All-Fluorescent White Organic Light-Emitting Diodes, *ACS Appl. Mater. Interfaces*, 2020, **12**, 16736–16742.

29 Y.-K. Wang, C.-C. Huang, S. Kumar, S.-F. Wu, Y. Yuan, A. Khan, Z.-Q. Jiang, M.-K. Fung and L.-S. Liao, The roles of thermally activated delayed fluorescence sensitizers for efficient red fluorescent organic light-emitting diodes with D-A-A type emitters, *Mater. Chem. Front.*, 2019, **3**, 161–167.

30 D. Zhang, X. Song, M. Cai and L. Duan, Blocking Energy-Loss Pathways for Ideal Fluorescent Organic Light-Emitting Diodes with Thermally Activated Delayed Fluorescent Sensitizers, *Adv. Mater.*, 2017, **30**, 1705250.

31 Y. Seino, H. Sasabe, Y. J. Pu and J. Kido, High-performance blue phosphorescent OLEDs using energy transfer from exciplex, *Adv. Mater.*, 2014, **26**, 1612–1616.

32 S. Y. Byeon, D. R. Lee, K. S. Yook and J. Y. Lee, Recent Progress of Singlet-Exciton- Harvesting Fluorescent Organic Light-Emitting Diodes by Energy Transfer Processes, *Adv. Mater.*, 2019, **31**, 1803714.

33 X. Hui, J. Zhang, D. Ding and Y. Wei, Extremely condensing triplet states of dpepo-type hosts through constitutional isomerization for high-efficiency deep-blue thermally activated delayed fluorescence diodes, *Chem. Sci.*, 2016, **7**, 2870–2882.

34 H. J. Jang and J. Y. Lee, Triplet energy boosting ternary exciplex host for improved efficiency in deep blue phosphorescent organic light emitting diode, *Org. Electron.*, 2019, **75**, 105441.

35 T.-A. Lin, T. Chatterjee, W.-L. Tsai, W.-K. Lee, M.-J. Wu, M. Jiao, K.-C. Pan, C.-L. Yi, C.-L. Chung, K.-T. Wong and C.-C. Wu, Sky-Blue Organic Light Emitting Diode with 37% External Quantum Efficiency Using Thermally Activated Delayed Fluorescence from Spiroacridine-Triazine Hybrid, *Adv. Mater.*, 2016, **28**, 7029.

36 Y. Zhang, M. Slootsky and S. R. Forrest, Enhanced efficiency in high-brightness fluorescent organic light emitting diodes through triplet management, *Appl. Phys. Lett.*, 2011, **99**, 223303.

37 X. Song, D. Zhang, Y. Zhang, Y. Lu and L. Duan, Strategically Modulating Carriers and Excitons for Efficient and Stable Ultrapure-Green Fluorescent OLEDs with a Sterically Hindered BODIPY Dopant, *Adv. Opt. Mater.*, 2020, **8**, 2000483.